

Inverse Compton Emission of TeV Gamma Rays from PSR B1259–63

J. G. Kirk^a Lewis Ball^b Olaf Skjæraasen^{b,1}

^a *Max-Planck-Institut für Kernphysik, Postfach 10 39 80, D-69029, Heidelberg,
Germany*

^b *Research Centre for Theoretical Astrophysics, University of Sydney, N.S.W.
2006, Australia*

Abstract

We derive light curves for the hard γ -ray emission, at energies up to several TeV, expected from the unique pulsar/Be-star binary system PSR B1259–63. This is the only known system in our galaxy in which a radio pulsar is orbiting a main sequence star. We show that inverse Compton emission from the electrons and positrons in the shocked pulsar wind, scattering target photons from the Be star, produces a flux of hard γ -rays that should be above the sensitivity threshold of present day atmospheric Cerenkov detectors. Furthermore, we predict that the flux of hard γ -rays produced via this mechanism has a characteristic variation with orbital phase that should be observable, and which is not expected from any other mechanism.

Keywords: Pulsars; inverse Compton scattering; gamma-rays; Cerenkov telescopes
PACS: 95.30Gv, 95.55KaX, 97.60Gb

1 Introduction

Pulsars are thought to lose their rotational energy by driving a relativistic wind of electrons, positrons and possibly ions. The radio pulsar PSR B1259–63 is in a binary system, and is orbiting a luminous, massive star [Johnston et al. 1996]. The orbit is highly eccentric ($e \sim 0.87$) and at periastron the pulsar is just $23R_*$ from its companion, a 10th magnitude B2e star, SS2883, of radius $R_* \sim 6R_\odot$ [Johnston et al. 1992, 1994].

¹ Institute of Theoretical Astrophysics, University of Oslo, P.O. Box 1029 Blindern, N-0315 Oslo, Norway

Observations indicate that this pulsar system is a source of unpulsed X-ray emission throughout its orbit [Hirayama et al. 1996]. The wind of PSR B1259–63 is likely to be confined by pressure balance with the strong Be-star outflow [Melatos, Johnston & Melrose 1995], and electrons and positrons will be accelerated and isotropised at the shock which terminates the relativistic pulsar wind. The observed X-ray emission has been interpreted as synchrotron emission from the shocked, relativistic electrons and positrons of the pulsar wind [Tavani & Arons 1997].

The high luminosity of the pulsar’s companion star, together with the relatively small separation of the binary, raises the possibility that the inverse Compton scattering of photons from the companion star by the relativistic electrons and positrons from the pulsar wind may be important. While the shocked electrons and positrons radiate synchrotron emission at energies in the X-ray band from keV to MeV, inverse Compton scattering of the photons from the Be star will produce high energy photons which are likely to be in the GeV to TeV range.

PSR B1259–63 is the only known galactic radio pulsar which is orbiting a main-sequence companion. Its spin down luminosity is 8.3×10^{28} W. If a fraction of 10^{-3} or more of this luminosity were converted into TeV photons via inverse Compton scattering, the flux at Earth would exceed the sensitivity threshold of imaging Cerenkov detectors such as that operated by the CANGAROO collaboration, which is $\sim 10^{-12}$ photons $\text{cm}^{-2} \text{s}^{-1}$ [Kifune et al. 1995]. The only other similar binary pulsar system, PSR J0045–73 [Kaspi et al. 1994, Bell et al. 1995], is in the Small Magellanic Cloud and is the most distant pulsar known. Although its binary separation at periastron is even smaller than that of PSR B1259–63, it is not likely to be observable in hard γ -rays because of its lower spin down luminosity and greater distance.

TeV γ -rays have been observed from the Crab nebula [e.g. Vacanti et al. 1991, HEGRA Collaboration 1996, Tanimori et al. 1998], and are attributed to inverse Compton scattering of self-produced synchrotron photons by electrons and positrons accelerated at the termination shock of a relativistic wind from the pulsar [De Jager & Harding 1992]. The emission from other pulsar nebulae that have been detected at TeV energies [see Kifune 1997 for a review] is attributed to inverse Compton scattering, by the shocked pulsar wind, of photons from the 2.7 K microwave background [Harding 1996]. None of the pulsars detected in hard γ -rays is in a binary system.

In the PSR B1259–63 binary system, photons from the Be star form the most important targets for inverse Compton scattering. The effect of this process on the distribution of synchrotron emitting electrons is included in the treatment of Tavani & Arons [1997]. However, they did not discuss the resulting γ -ray emission. In this paper we compute both the synchrotron and inverse

Compton flux emitted by the electrons and positrons accelerated at the termination shock of the relativistic wind of PSR B1259–63, as a function of the orbital phase of the binary. The highly energetic inverse Compton photons may be absorbed by photon-photon pair creation whilst propagating through the radiation field of the companion star, and the effective optical depth due to this process is included in our calculations. The parameters which describe the pulsar wind are determined approximately from the observed X-ray fluxes near periastron, and the model is then used to predict the light curves at energies from 100 MeV to 1 TeV. The modelling indicates that it may be possible to detect PSR B1259–63 using an imaging Cerenkov detector such as that operated by the CANGAROO collaboration. To date, only a limited number of observations of this object have been made using this telescope, with the possibility of at best a marginal detection [Sako et al. 1997, Patterson & Edwards, private communication]. We show that the inverse Compton scattering of Be-star photons produces an unambiguous variation in the hard γ -ray flux which should be observable, and which is unlikely to result from any other mechanism.

2 Emission from a shocked pulsar wind

The wind of the Crab pulsar is thought to have a Lorentz factor of $\Gamma \approx 10^6$, and to terminate at a collisionless shock front situated some 3×10^{15} m from the neutron star where it attains pressure balance with the surrounding material [Rees & Gunn 1974]. In the Kennel & Coroniti [1984] model of the Crab nebula, the pulsar wind electrons are accelerated at this shock front and the kinetic energy of the wind is converted into a power-law distribution of electrons extending over several decades in energy. (Note that when used alone, the term ‘electron’ can be taken to refer to both electrons and positrons in the pulsar wind.) The synchrotron emission from these particles is detected at all frequencies from the radio regime to γ -rays of energies up to 10 GeV. Gamma-rays of higher energy are believed to be produced by a synchrotron self Compton process whereby the shocked synchrotron-emitting electrons inverse Compton scatter synchrotron photons at infrared to optical frequencies [De Jager & Harding 1992].

Following Kennel & Coroniti [1984], we assume that the shock front that terminates the wind of PSR B1259–63 accelerates the electrons incident upon it and injects them into the downstream region such that when integrated over the shock surface, the injection rate is isotropic in the rest frame of the pulsar, and is a power-law in momentum extending from a lower limit γ_1 to an upper limit γ_2 .

The injection rate in an interval $d\gamma$, integrated over solid angle, is $Q_e(\gamma)d\gamma$

where

$$Q_e(\gamma) = \begin{cases} Q_0 \gamma^{-q} & \text{for } \gamma_1 < \gamma < \gamma_2, \\ 0 & \text{otherwise.} \end{cases} \quad (1)$$

Assuming that the unshocked pulsar wind contains monoenergetic electrons and positrons of Lorentz factor Γ , one can eliminate two of the three free parameters Q_0 , γ_1 and γ_2 in terms of Γ and that fraction η of the pulsar luminosity L_p which is channelled into relativistic electrons: ηL_p . Using the dynamic range $\rho = \gamma_2/\gamma_1$ as the remaining free parameter, one finds:

$$\gamma_1 = \Gamma \left(\frac{q-2}{q-1} \right) \left[\frac{1-\rho^{1-q}}{1-\rho^{2-q}} \right] \quad (2)$$

which depends only weakly on ρ for $q > 2$ and $\rho \gg 1$. Energy conservation implies

$$Q_0 = \gamma_1^{q-1} \frac{\eta L_p}{\Gamma m c^2} \frac{(q-1)}{1-\rho^{1-q}}. \quad (3)$$

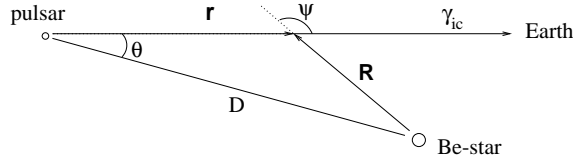


Fig. 1. Sketch of the binary system defining angles and distances used in the text.

For the purpose of calculating the inverse Compton emissivity of an electron, we assume that the spectrum of the pulsar's companion star can be approximated as monochromatic at frequency $\nu_0 = 2.7k_B T_{\text{eff}}/h$, where T_{eff} is the effective temperature of the star [Blumenthal & Gould 1970]. We denote by $n_\gamma(\epsilon, \vec{R}, \vec{\Omega}) d\vec{\Omega} d\epsilon$ the differential number density of target photons moving within the solid angle $d\vec{\Omega}$ of the unit vector $\vec{\Omega}$ at position \vec{R} with respect to the star, with energy between $E = \epsilon m c^2$ and $(\epsilon + d\epsilon)m c^2$ where ϵ is dimensionless and m is the electron mass. Then

$$n_\gamma(\epsilon, \vec{R}, \vec{\Omega}) = N(R) \delta(\epsilon - \epsilon_0) \delta(\vec{\Omega} - \hat{\vec{R}}) \quad (4)$$

where $N(R) = L_*/(4\pi R^2 c h \nu_0)$ is the photon density, $\epsilon_0 = h\nu_0/mc^2$ is the dimensionless energy of the Be-star photons, $\hat{\vec{R}} = \vec{R}/R$ is a unit vector, and L_* is the stellar luminosity.

The ratio of emission due to synchrotron losses to that due to inverse Compton losses is, in the classical limit, determined by the relative energy density in the magnetic field and in the target photons. It is therefore convenient to introduce the parameter

$$b \equiv \sqrt{\frac{B^2/8\pi}{h\nu_0 N}}. \quad (5)$$

We assume that the pulsar-shock separation is small compared with the pulsar-Be star separation D . In this case, both the target photon density, $N \approx N(D)$, and the angle between the line of sight and the direction of the target photons, ψ , remain constant over the shock surface. The (isotropic) electron distribution function, integrated over the entire source can be easily derived from the kinetic equation in two special cases. If adiabatic losses dominate, the shape of the spectrum is unchanged by the losses and one can approximate the distribution function as a product of the loss time and the injection function:

$$n_e(\gamma) = \Delta t Q_e(\gamma). \quad (6)$$

If, on the other hand, radiative losses dominate, the kinetic equation [e.g. Eq. 56 of Tavani & Arons 1997] is easily solved to give:

$$\begin{aligned} n_e(\gamma) &= \frac{1}{\langle -\dot{\gamma}_{ic} \rangle + \langle -\dot{\gamma}_s \rangle} \int_{\gamma}^{\infty} \frac{d\gamma'}{4\pi} Q_e(\gamma') \\ &= \begin{cases} \frac{Q_0}{4\pi(q-1)} \frac{(\gamma^{1-q} - \gamma_2^{1-q})}{(\langle -\dot{\gamma}_{ic} \rangle + \langle -\dot{\gamma}_s \rangle)} & \text{for } \gamma_1 < \gamma < \gamma_2, \\ \frac{Q_0}{4\pi(q-1)} \frac{(\gamma_1^{1-q} - \gamma_2^{1-q})}{(\langle -\dot{\gamma}_{ic} \rangle + \langle -\dot{\gamma}_s \rangle)} & \text{for } \gamma < \gamma_1. \end{cases} \end{aligned} \quad (7)$$

The quantity $\langle \dot{\gamma}_{ic} \rangle$ is the rate of change of the electron Lorentz factor due to inverse Compton losses, averaged over scatterings and over an isotropic distribution of electron directions (or equivalently, of incoming photon directions). Similarly, $\langle \dot{\gamma}_s \rangle$ is the corresponding quantity for synchrotron losses, averaged over pitch angle. In deriving Eq. (7) we have used the continuous approximation to the inverse Compton losses [Blumenthal 1971] and ignored triplet pair production, since the maximum value of the parameter γ_{ϵ_0} which we consider is of order 500 [Mastichiadis 1991]. The details of the calculations of $\langle \dot{\gamma}_{ic} \rangle$ and $\langle \dot{\gamma}_s \rangle$ are presented in Appendix A.

The rate at which the electrons emit inverse Compton photons per steradian per second per energy interval depends on the angle ψ of Fig. 1 and is given by

$$\frac{dN_{ic}}{d\vec{\Omega}d\epsilon dt} = \int d\gamma n_e(\gamma) \eta_{ic}(\epsilon, \gamma, \psi) \quad (8)$$

where $\eta_{ic}(\epsilon, \gamma, \psi)$ is the inverse Compton emissivity – the number of photons emitted per second per electron in unit energy interval around ϵ . Analogously, the corresponding synchrotron emission depends on the angle between the

magnetic field in the source and the line of sight. This, however, is likely to vary considerably through the source, so that we average over all pitch-angles:

$$\frac{dN_s}{d\vec{\Omega}d\epsilon dt} = \int d\gamma n_e(\gamma) \eta_s(\epsilon, \gamma) \quad (9)$$

where $\eta_s(\epsilon, \gamma)$ is the synchrotron emissivity. The details of the calculation of the rates of emission are presented in Appendix A.

Photons of sufficiently high energy produced by inverse Compton scattering, may interact with the radiation field of the Be star on their way from the source to the observer and create electron-positron pairs, $\gamma\gamma \rightarrow e^+e^-$. If a substantial fraction of the inverse Compton emission is absorbed, an electron positron pair cascade will result and the power will emerge at lower photon energy in a beaming pattern which is likely to be reasonably isotropic. However, this effect should not overwhelm the primary radiation from the shocked electrons close to the neutron star, since the reradiated power occupies a larger solid angle than the intercepted power and the primary radiation itself is in general more intense at lower photon energy. To a first approximation, therefore, we treat this effect as absorption. The derivation of the effective optical depth due to pair-production, $\tau(\epsilon, \theta)$, is presented in Appendix B. The minimum energy required for pair creation via this process is

$$\epsilon_{ic} \geq 2/[(1 - \cos \psi)\epsilon] \quad (10)$$

which corresponds to roughly $51 \text{ GeV} \times 2/(1 - \cos \psi)$ for the assumed monochromatic Be-star spectrum.

We denote by F_E the total observed energy flux per unit energy interval due to synchrotron and inverse Compton emission from the shocked, accelerated electrons and positrons. When corrected for the absorption by pair-production on Be-star photons, one has

$$EF_E = \frac{\epsilon^2 mc^2}{d^2} \left(\frac{dN_s}{d\vec{\Omega}d\epsilon dt} + \frac{dN_{ic}}{d\vec{\Omega}d\epsilon dt} \right) e^{-\tau}, \quad (11)$$

where d is the distance to the emission region.

3 Application to PSR B1259–63

The published observations available to constrain the parameters consist of a set of four detections at different epochs by the ASCA satellite [Kaspi et al. 1995, Hirayama et al. 1996], a single set of measurements by the OSSE experiment [Grove et al. 1995] taken over a range of epochs, and upper limits

from the COMPTEL and EGRET experiments [Tavani et al. 1996]. In addition, the source has been detected at an epoch far from periastron by the ROSAT satellite [Cominsky, Roberts & Johnston 1994], but the measurement is not sufficiently precise to constrain the model significantly, and will not be discussed here.

The emission in the range 2 – 10 keV (ASCA) varies with orbital phase close to periastron. Of the four epochs measured, that closest to periastron stands out from the other three because the flux is approximately a factor of two weaker and the spectrum significantly softer. The sensitivity of the OSSE experiment is not sufficient to detect such variability in the 50 – 200 keV band. We therefore consider the OSSE observations as an average over epochs spread over about 20 days around periastron.

The most obvious constraint on the model is given by the very hard photon index of roughly -1.7 measured by ASCA and OSSE and consistent with the relative intensities of the fluxes in the two bands. In the shock acceleration picture, the X-ray emission can be interpreted as either inverse Compton or synchrotron emission. However, the inverse Compton interpretation would require a very low value for the Lorentz factor of the pulsar wind ($\Gamma \sim 500$), compared to that derived for the Crab pulsar ($\Gamma \sim 10^6$), in order to satisfy the upper limits imposed by the EGRET measurements. We do not consider the inverse Compton interpretation of the X-ray emission further here.

The first fundamental question to be answered before attempting a fit to the spectrum is whether the accelerated electrons are able to cool radiatively (by synchrotron emission or inverse Compton emission), or whether they first lose their energy by adiabatic losses in the post-shock flow. Ball et al. [1998] estimate a field of ~ 1 G at the shock at periastron, in which case electrons with a Lorentz factor of 10^6 radiate synchrotron emission in the X-ray band and have a synchrotron half life time of roughly 10 minutes. A simple estimate of the timescale associated with the flow patterns – and thus the adiabatic losses – is that it is the stand-off distance of the pulsar wind shock, divided by the post-shock speed. For an ultrarelativistic flow such as is thought to emerge from the pulsar, the post-shock speed is $c/3$. On the other hand, the stand-off distance of the pulsar wind shock is likely to scale with the distance between the stars. We therefore approximate the timescale for adiabatic losses as

$$\Delta t = f3D/c, \tag{12}$$

where $f \ll 1$ to conform with our assumption that the emission region is always situated close to the pulsar. Taking $f = 0.1$ leads to a Δt of roughly 2 minutes close to periastron and ~ 22 minutes at apastron. Thus it is by no means clear which loss mechanism – radiative or adiabatic – dominates. Since we do not attempt to model the flow pattern, we present both possibilities, bearing in mind that the real system might lie in an intermediate region.

Another fundamental question concerns the orbital variation of the magnetic field strength in the radiating region. The position of the pulsar wind shock is thought to be determined by a balance between the ram pressures of the Be-star wind and the pulsar wind [Melatos, Johnston & Melrose 1995], which might reasonably be expected to vary throughout the orbit. To characterise the resulting variation in the magnetic field strength, we adopt a simple scaling: we assume that the parameter b of Eq. (5) – the ratio of the energy density in the magnetic field to that in the Be-star’s radiation field in the emission region – is constant. This is the case, for example, if the distance of the shock from both the pulsar and the Be star is proportional to the separation of the two stars, and if the magnetic field associated with the pulsar has a $1/r$ dependence. Such a distance scaling in its turn results if the radial dependence of the ram pressures of the two winds is the same (for example $1/r^2$).

Table 1

Parameters for the PSR B1259–63 system. References are: 1–Johnston et al. [1996]; 2–Johnston et al. [1994]; 3–Underhill & Doazan [1982].

Parameter		Value	Reference
Pulsar			
period	P	47.762 ms	1
period derivative	\dot{P}	2.279×10^{-15}	1
surface magnetic field	B_p	3.3×10^7 T	1
spin down luminosity	L_p	8.3×10^{28} W	1
Be star			
spectral type		B2	2
effective temperature	T_{eff}	2.28×10^4 K	3
radius	R_*	$6.0R_\odot = 4.2 \times 10^9$ m	3
luminosity	L_*	$8.8 \times 10^3 L_\odot = 3.3 \times 10^{30}$ W	3
effective photon energy	ϵ_0	$2.7k_B T_{\text{eff}}/(mc^2) = 10^{-5}$	
mass	M_*	$10M_\odot = 2 \times 10^{31}$ kg	3
System			
eccentricity	e	0.87	1
periastron separation	D_τ	$23R_* = 9.6 \times 10^{10}$ m	
apastron separation	D_a	$331R_* = 1.4 \times 10^{12}$ m	
orbital inclination	i	35°	1
orbital period		1236.8 days	2
distance	d	1.5 kpc	1

3.1 Adiabatic losses

The simplest case to discuss is that in which adiabatic losses rapidly quench the synchrotron and inverse Compton emission. Since adiabatic losses do not alter the slope of the electron distribution, we can approximate their effect as one of switching off the synchrotron and inverse Compton radiation after a finite time interval Δt which is short compared to a radiative cooling time. The electron density in the emission region is then given by Eq. (6), and the only orbital variation in the emitting distribution enters through the adiabatic loss time (Eq. 12), in which we have set $f = 0.1$.

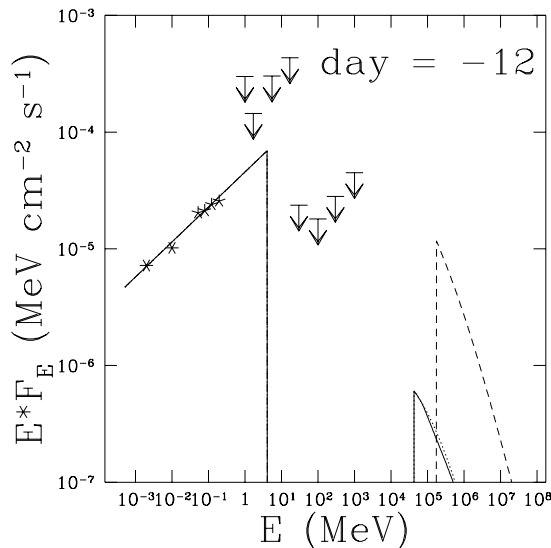


Fig. 2. Model spectrum 12 days prior to periastron when adiabatic losses dominate. The solid line shows the emission for $b = 1$ ($B = 3.2$ G), and the dotted line depicts the intrinsic emission, uncorrected for photon-photon absorption. The dashed line shows the inverse Compton emission for $b = 0.1$ ($B = 0.32$ G) with injection rescaled to give the same synchrotron emission as the higher field case. Detections by ASCA and OSSE are shown as asterisks, and the upper limits are from COMPTEL and EGRET.

The photon index of -1.7 is matched in this case by injecting electrons with a power-law index $q = 2.4$, close to that which is thought to be produced in the Crab nebula. In Fig. 2 we show a model spectrum computed for an epoch 12 days prior to periastron; the model parameters for this and subsequent figures are given in Table 2. Also shown in this figure are the fluxes observed at the same epoch by ASCA, together with the observations by OSSE and the upper limits from the COMPTEL and EGRET experiments. The sharp cut-off of the synchrotron emission above about 5 MeV and of the inverse Compton emission below about 50 GeV is an artifact of two of our approximations: that of sharp cut-offs at γ_1 and γ_2 in the electron injection spectrum, and the ‘delta-function’ approximation to the emissivities. Replacing the delta-

function emissivities with the correct forms rounds off these cut-offs but does not change our conclusions. Perhaps the most striking aspect of the model fit is the importance of the EGRET upper limits in constraining the upper extent of the synchrotron emission. One can immediately deduce that

$$10^{15} < \gamma_2^2 B < 10^{17} \quad (13)$$

where B is measured in gauss. In addition, it can readily be seen that the electron injection function must be close to a power law over at least a decade of γ in order to fit the observations, as stressed by Grove et al. [1995].

Table 2

Parameters for the models presented in Figs. 2–8. b is the square root of the ratio of magnetic to radiation energy density in the source, q the power-law index of the electron injection function, Γ the Lorentz factor of the pulsar wind, η the efficiency of conversion of spin-down power into injected electrons and ρ the range of Lorentz factors over which injection occurs, γ_2 being the upper cut-off.

Figure	Model parameters						
	b	q	Γ	η	ρ	Losses	Implied γ_2
2, 3	1	2.4	5×10^5	4.4×10^{-4}	100	adiabatic	1.7×10^7
2	0.1	2.4	1.6×10^6	1.4×10^{-2}	100	adiabatic	5.4×10^7
4, 5	1	1.2	2×10^6	1.3×10^{-2}	100	radiative	1.2×10^7
6, 7, 8	0.1	1.4	5×10^6	1.5×10^{-2}	100	radiative	4.3×10^7

Since in this case the electron distribution is not influenced by radiative losses, the synchrotron emission is unaffected by a change in the magnetic field strength, provided the upper and lower cut-offs of the injection spectrum (γ_1 and γ_2) and the absolute level of emission (i.e., η) are appropriately rescaled. The resulting inverse Compton emission, on the other hand, is strongly affected by the choice of b . In Fig. 2, the solid line shows the emission 12 days prior to periastron, computed under the assumption that the energy density in the magnetic field equals that in Be-star photons at the position of the pulsar, i.e., $b = 1$, which corresponds to a field strength of 3.2 G at this epoch. The substantially larger inverse Compton flux depicted by the dashed line is that which results from a model which produces the same synchrotron emission but has $b = 0.1$, corresponding to $B = 0.32$ G. The inverse Compton emission increases by considerably less than a factor b^{-2} because of the Klein-Nishina effects.

At energies above about 50 GeV, the spectrum is affected by absorption due to photon-photon pair production in the radiation field of the Be star. We show this explicitly in Fig. 2 by plotting the intrinsic emission, without allowance for absorption, as a dotted line.

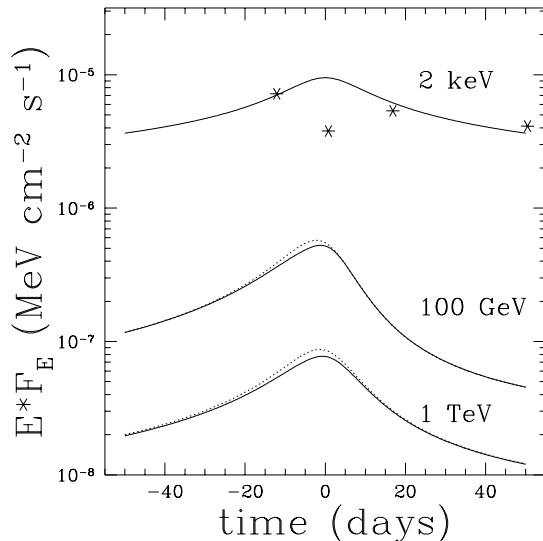


Fig. 3. Model light curves in the X-ray and γ -ray bands around periastron when adiabatic losses dominate. The abscissa gives the time in days relative to periastron. The solid lines show the emission for $b = 1$, for the same parameters as in Fig. 2, and the dotted lines depict the intrinsic emission, uncorrected for photon-photon absorption.

The light curves in the X-ray and hard γ -ray bands, when adiabatic losses dominate, are depicted in Fig. 3. There is no emission between about 5 MeV and 50 GeV in this case for two reasons: firstly, because there is a lower limit to the energy at which electrons are injected, and secondly, our crude treatment of adiabatic losses simply switches off emission after a finite time and does not model the cooling of electrons to energies below the lower injection cut-off. The observations by ASCA are indicated by asterisks and are to be compared to the 2 keV light curve. The increase in the model light curve at 2 keV is clearly contradicted by the observations. This point has been discussed in detail by Tavani & Arons [1997], and we return to it in the following section. The behaviour of the model is the result of two competing effects. Firstly, the assumption of constant b implies that the magnetic field in the emission region is inversely proportional to the separation of the stars. For a fixed power-law electron distribution, the emission at a given frequency increases according to $B^{(q+1)/2}$. Folding this with the assumed dependence of Δt , we find the emission varies as $D^{(1-q)/2}$. With $q = 2.4$, the increase in emission between -12 days and periastron is about a factor of 1.3.

Although the X-ray light curve does not fit the observations, the inverse Compton light curves display interesting features which persist in the more complicated cases in which radiative cooling dominates. Since b is assumed constant over the orbit, the ratio of inverse Compton to synchrotron luminosity is approximately constant. However, the inverse Compton radiation is anisotropic, being stronger when the target photons are scattered head-on into the line of

sight, than when they are deflected by an angle of less than 90° . The scattering angle ψ is a function of orbital phase, and, because of the inclination of the orbit, it is larger before periastron than after. This accounts for the asymmetry of the flux evolution at 100 GeV with respect to periastron. The 100 GeV emission is systematically stronger before periastron, reaching a maximum close to the point at which the scattering angle peaks, at -6.4 days. The same behaviour is displayed by the intrinsic (unabsorbed) emission at 1 TeV (dotted line). However, the largest scattering angle is achieved when the pulsar is almost ‘behind’ the star, at which point the optical depth along the line of sight due to absorption by photon-photon pair production is greatest. This effect reduces the emerging flux at 1 TeV just prior to periastron. Nevertheless, its value 20 days before periastron is about a factor of 1.5 larger than 20 days after periastron.

3.2 Radiative losses

When radiative losses dominate over adiabatic losses, the shape of the electron distribution function varies with orbital phase, because the loss terms $\langle \dot{\gamma}_{ic,s} \rangle$ are functions of γ and depend on the stellar separation. Assuming that the timescale associated with the orbital motion is much longer than the radiative loss timescale, the instantaneous values of the loss terms can be inserted into Eq. (7) to find the electron distribution.

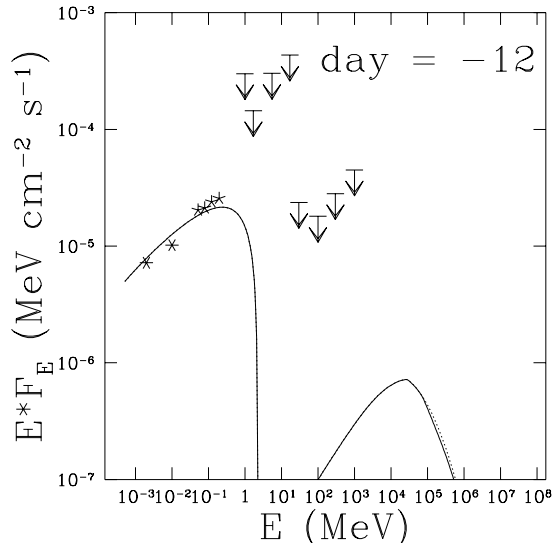


Fig. 4. Model spectrum 12 days prior to periastron when radiative (synchrotron) losses dominate. The solid line shows the emission for $b = 1$ ($B = 3.2$ G), and the dotted line depicts the intrinsic emission, uncorrected for photon-photon absorption. Detections by ASCA and OSSE are shown as asterisks, and the upper limits are from COMPTEL and EGRET.

The synchrotron loss timescale is inversely proportional to the electron Lorentz factor γ throughout the entire spectrum. Consequently, when synchrotron losses dominate, the observed (photon) spectral index is $-(q + 2)/2$. The photon index of -1.7 measured by ASCA and OSSE can therefore be reproduced by choosing an injection spectrum with $q = 1.4$. However, such a hard injection spectrum displays a much broader ‘roll-over’ in the neighbourhood of the upper cut-off, as can be seen from Eq. (7). Compensating for this with an even harder injection spectrum gives a better fit to the OSSE observations, as is shown in Fig. 4. Here we have chosen $b = 1$, so that, because the Klein-Nishina effects weaken the inverse Compton losses, synchrotron cooling dominates. The synchrotron emission is similar to that of Fig. 2, except for the smooth roll-over. However, the inverse Compton emission contains a new, rather weak, component in the EGRET waveband. This arises from electrons which have cooled to Lorentz factors lower than the minimum at which injection took place, γ_1 . The photon index in this band is -1.5 , appropriate to cooling electrons which were all injected at higher energy.

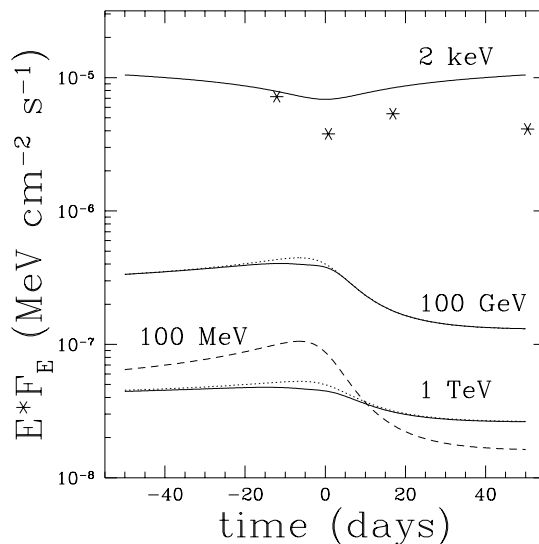


Fig. 5. Model light curves in the X-ray and γ -ray bands around periastron when radiative (synchrotron) losses dominate. The solid lines show the emission for $b = 1$, for the same parameters as in Fig. 4. The dotted lines depict the intrinsic emission, uncorrected for photon-photon absorption. Note that the emission at 100 MeV was not present in the adiabatically cooled case (Fig. 2).

The corresponding light curves are shown in Fig. 5. The light curve at 2 keV now displays a slight dip at periastron, in contrast to the case where adiabatic losses dominate shown in Fig. 3. This demonstrates the changes in the shape of the electron distribution with orbital phase. The total emitted luminosity is independent of orbital phase because the efficiency η of conversion of pulsar spin-down luminosity to relativistic electrons is held constant, and because essentially all of the energy in the electrons is radiated. The relative importance of synchrotron and inverse Compton emission is controlled by the

parameter b , which is also constant, so that the synchrotron luminosity does not vary with phase. However, since the magnetic field in the source region is stronger at periastron, electrons radiate at higher frequencies there, i.e., the entire spectrum in the EF_E plot shown in Fig. 4 is shifted horizontally to the right. The size of the effect this has on the light curve at 2 keV depends on the spectral index. The observed dip by roughly a factor of 2 would require a change of one order of magnitude in the magnetic field, given the observed photon index of -1.7 . In our model the magnetic field increases by only a factor of 1.5 between the epoch -12 days and periastron, giving a change of only 14% in the flux.

As in the case when adiabatic losses dominate, the γ -ray emission is sensitive to a change in the parameter b . The inverse Compton loss timescale is inversely proportional to γ for very low Lorentz factors $\gamma\epsilon_0 \ll 1$. However, unlike the synchrotron case, Klein-Nishina corrections weaken the losses at higher γ until, at about $\gamma\epsilon_0 \approx 1$ (corresponding to $\gamma \approx 10^5$ here), the timescale becomes independent of γ . This behaviour significantly complicates the resulting spectrum, since for electrons radiating synchrotron emission in the X-ray band, $\gamma\epsilon_0 > 1$. Where inverse Compton losses dominate, the electron distribution tends to have the same power law index as the injection spectrum, and the photon index of synchrotron emission from these electrons is thus ~ 0.5 harder than that produced where synchrotron cooling dominates. As the magnetic field is reduced, inverse Compton cooling first starts to dominate at the low frequency end of the spectrum since the weakening due to Klein-Nishina effects is not strongly pronounced there. This tends to give a harder spectrum in the ASCA range than in the OSSE range.

An example of this effect is shown in Fig. 6, where we have chosen the parameter $b = 0.1$. As in the case where adiabatic losses dominate, the inverse Compton flux level is higher than for the stronger field case shown in Fig. 4, and is now comparable to that of the synchrotron emission. However, the synchrotron spectrum now has a pronounced turnover at low energies and its shape is quite different to that shown in Fig. 4. In order to compensate for the hardening effect of the inverse Compton cooling, the fit presented in Fig. 6 used an injection spectrum with $q = 1.4$, softer than the injection spectrum with $q = 1.2$ used for Fig. 4. The harder model spectrum in the ASCA range has a marked effect on the light curve, which is shown in Fig. 7. The flux at 2 keV is now much more sensitive to a shift of the emission to higher frequency, and therefore the dip in flux at periastron is more pronounced.

Despite the strong difference in the behaviour of the X-ray light curve in the cases where adiabatic and radiative losses dominate, the characteristics of the γ -ray curves are essentially the same. This is due in the first place to the effect of the scattering angle, which has the same orbital dependence in both cases. In the second place, the photon index in the γ -ray range is much softer when

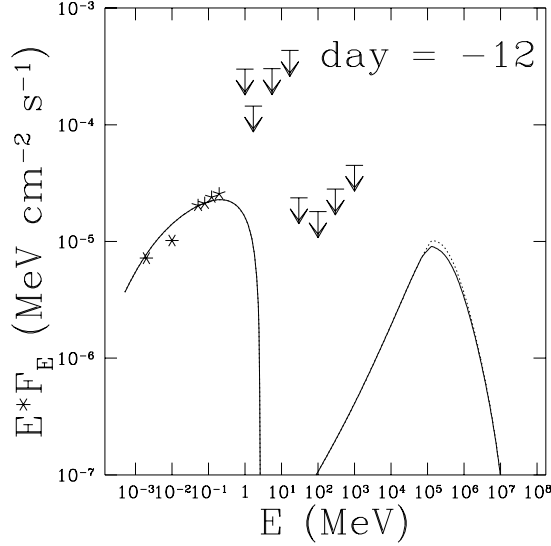


Fig. 6. Model spectrum 12 days prior to periastron when radiative (inverse Compton) losses dominate. The solid lines show the emission for $b = 0.1$ ($B = 0.32$ G), and the dotted line depicts the intrinsic emission, uncorrected for photon-photon absorption. Note the curvature of the spectrum at energies between 1–10 keV which results from inverse Compton losses.

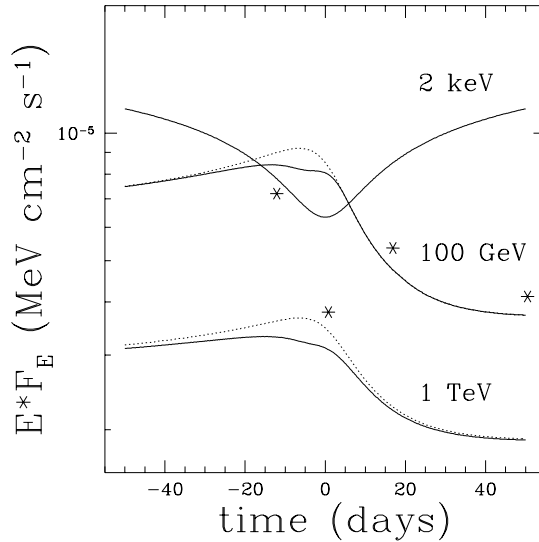


Fig. 7. Model light curves in the X-ray and γ -ray bands around periastron when radiative (inverse Compton) losses dominate. The solid lines show the emission for $b = 0.1$, for the same parameters as in Fig. 6. The dotted lines depict the intrinsic emission, uncorrected for photon-photon absorption.

radiative losses dominate, and this tends to enhance the emission when the spectrum is boosted to higher frequencies, whereas it decreases the emission at 2 keV. In the adiabatic case, where the luminosity is not fixed, the increased photon density at periastron causes a rise in the inverse Compton flux, whilst

at the same time the stronger magnetic field causes a rise in the synchrotron flux (see Fig. 3).

Fig. 8 shows the light curve of Fig. 7 extended over the entire orbit. According to our model, X-ray emission should persist at all epochs. This is in agreement with the ROSAT detection near apastron [Cominsky, Roberts & Johnston 1994], although the observed flux was rather lower than the model flux. The most prominent feature of the light curves is the steady increase in γ -ray emission from soon after one periastron to just prior to the next periastron. This mirrors the dependence of the inverse Compton radiation mechanism on the angle between the line of sight and the vector connecting the stars.

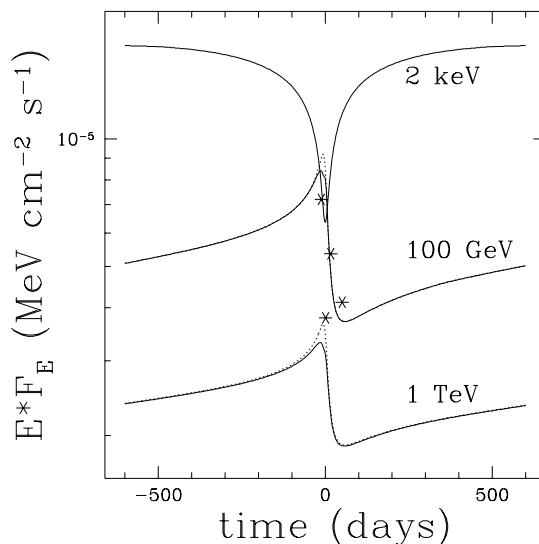


Fig. 8. The model light curves of Fig. 7 extended to cover the entire orbit.

4 Discussion

In presenting models of the high energy emission from shock accelerated electrons in PSR B1259–63 we have used simple scaling rules for those quantities which depend on the flow pattern of plasma in this binary system. Thus, the stand-off distance of the pulsar wind termination shock is the basic length scale governing the importance of adiabatic losses, and we assume that the ratio of this length to the stellar separation is constant. It is clear from the unpulsed radio emission detected from the system near periastron that the pulsar interacts with a disk around the Be star [Ball et al. 1998]. Nevertheless, we have assumed that the position of the termination shock is not affected by the disk, and have also taken the magnetic field strength at the shock front as well as the density in target photons from the Be star to be unchanged by the presence of the disk. In this case a $1/r$ dependence of the magnetic field

together with the $1/R^2$ dependence of the photon density (see Fig. 1) ensures that the ratio of the energy density in the magnetic field to that in the target photons is independent of orbital phase.

These approximations are plausible except when the pulsar is very close to periastron. Changes in the observed pulsed radio emission [Johnston et al. 1996] and observations and interpretation of the unpulsed radio emission seen around periastron [Johnston et al. 1998, Ball et al. 1998], imply that the interaction of the pulsar wind and the Be-star disk is confined to the period from about day -25 to $+25$. There are few observational data of X-ray and γ -ray emission available at epochs outside this range. We have therefore made comparisons of our model predictions with observations taken close to periastron. The models presented indicate the trends produced by effects such as the competition between synchrotron and inverse Compton cooling. In particular, our results indicate that the influence of inverse Compton cooling on the spectral index in the X-ray band is strongly affected by the functional dependence of the Klein-Nishina corrections on the electron Lorentz factor. However, they cannot be expected to accurately fit the observations made close to periastron.

In common with most discussions of particle acceleration at pulsar wind termination shocks [e.g. Kennel & Coroniti 1984], we assume that the mechanism produces a featureless power-law distribution between two sharp cut-offs. In reality, the upper cut-off is likely to be determined by competition between radiative losses and acceleration, which may set in fairly sharply in energy space if the acceleration rate is a decreasing function of Lorentz factor and losses are increasing. The lower cut-off, on the other hand, depends on the mechanism by which some electrons from the relativistic MHD wind are decelerated, and the physical basis for the assumption of a sharp lower cut-off is unclear. These uncertainties should be kept in mind when judging the results of detailed spectral modelling.

All of the models that we have presented require that only a small fraction ($\sim 1\%$) of the pulsar spin down luminosity be radiated by the shocked electrons and positrons of the pulsar wind. The efficiencies are comparable to those inferred for the Crab nebula [De Jager & Harding 1992] and are in agreement with those suggested by Tavani & Arons [1997]. They are consistent with the likelihood that ions carry much of the wind luminosity and that a large fraction of the power is used to drive the expansion of the nebula. The value of ϵ_0 that we have used, together with the high Lorentz factor of the unshocked pulsar wind, means that the inverse Compton scattering is well into the Klein-Nishina regime. If the energy of the target photons is somewhat lower, then the absorption due to pair production would be larger (albeit above a higher threshold energy) and the orbital variation of the hard γ -ray flux would be larger than shown in our model light curves.

The problem of fitting the X-ray observations close to periastron has been thoroughly discussed by Tavani & Arons [1997], and the properties of the flow pattern, not considered in our work, play a crucial role in their analysis. The reduction of the flux at 2 keV and simultaneous spectral softening at periastron seen by ASCA is reproduced by taking account of the competition between adiabatic and radiative losses and by adopting strong shielding (or shadowing) of the emission region from the target photons whilst the pulsar is traversing the Be-star disk, (assumed to be whenever the orbital phase is outside the range $-50^\circ < \phi < 50^\circ$). The strong inverse Compton cooling which sets in upon emergence into the full photon flux within a few days of periastron is responsible for both transferring emission out of the X-ray band into the γ -ray region and softening the electron distribution. The details of the conclusions reached by Tavani & Arons [1997] may be modified by the dependence of the Klein-Nishina corrections on the electron energy which we have shown to be important. Calculations of models which include both the flow pattern and the full functional form of the Klein-Nishina corrections are warranted.

Our results show that the γ -ray emission is not sensitive to the modelling of the X-ray flux close to periastron. The major parameter governing the expected γ -ray intensity is the magnetic field strength, and the values we have adopted are relevant to the PSR B1259–63 system [Ball et al. 1998]. The spectral index in the 100 GeV to TeV range is generally much softer than in X-rays because of the fall-off of the Klein-Nishina cross section at high energy, but the fluxes we predict are of the order of 10^{-10} photons $\text{cm}^{-2} \text{s}^{-1}$ at 100 GeV – well above the sensitivity threshold of proposed Cerenkov imaging telescopes [Kawachi 1997]. The light curve of these γ -rays is affected in the TeV range by absorption on Be-star photons, but at lower energies is dominated by the change of scattering angle through the orbit, an effect which should appear whenever the pulsar is out of the shadow of the Be-star disk, i.e., over almost the entire orbit. Other production mechanisms, such as the decay of π^0 particles produced in nuclear collisions, or the inverse Compton scattering of synchrotron photons or of photons from the microwave background, are expected to give isotropic emission. Any variation of the flux produced by these mechanisms should then be symmetric about periastron. Detection of an asymmetric variation, such as we predict, of the hard γ -ray flux from PSR B1259–63 would provide conclusive proof that inverse Compton scattering of the Be-star photons is the responsible radiation mechanism.

Acknowledgements

We thank Simon Johnston for finding this pulsar, and for many helpful discussions. Our collaboration was made possible by support for J.K. from the RCfTA, University of Sydney, under its international visitor programme and

for L.B. from the MPIK Heidelberg. O.S. thanks the RCfTA, University of Sydney, for its support during work on this project, and the Norwegian Research Council for support of this work through a postgraduate grant.

Appendix A: Inverse Compton and synchrotron emissivities

An electron of Lorentz factor γ scatters target photons at an average rate

$$\dot{N}_{\text{ic}} = c \int d\vec{\Omega} \int d\epsilon \frac{\epsilon'}{\gamma\epsilon} n_{\gamma}(\epsilon, \vec{R}, \vec{\Omega}) \sigma_{\text{KN}}(\epsilon') \quad (14)$$

[Jones 1965], where ϵ is the energy of the target photon, ϵ' is the energy of the target photon seen in the electron rest frame and $\sigma_{\text{KN}}(x)$ is the Klein-Nishina cross section. On inserting (4) into Eq. (14) one finds

$$\dot{N}_{\text{ic}} = cN(R) \sigma_{\text{KN}}(\epsilon') \frac{\epsilon'}{\gamma\epsilon_0}. \quad (15)$$

For an electron moving at an angle ψ to \vec{R} , one has

$$\epsilon' = \gamma\epsilon_0(1 - \beta \cos \psi) \quad (16)$$

where $c\beta$ is the speed of the electron, and thus the scattering rate depends implicitly on the direction of motion of the electron relative to that of the photon, and so $\dot{N}_{\text{ic}}(\gamma, \psi)$.

The rate of change of electron energy averaged over scatterings remains a function of the direction of motion, and is given by [Jones 1965],

$$\dot{\gamma}_{\text{ic}}(\gamma, \psi) = -\frac{3}{8} cN(R) \sigma_{\text{T}} \frac{\epsilon'^2}{\epsilon_0} \left(1 - \frac{\epsilon_0}{\epsilon'\gamma} - \frac{\epsilon_0}{\gamma} \right) F_{\text{loss}}(\epsilon') \quad (17)$$

where σ_{T} is the Thomson cross section and

$$F_{\text{loss}}(x) = \int_0^2 df \frac{f(f^2 - 2f + 2)}{(1 + xf)^3} \left[1 + \frac{(xf)^2}{(f^2 - 2f + 2)(1 + xf)} \right] \quad (18)$$

which can be integrated by elementary techniques, to give

$$F_{\text{loss}}(x) = \frac{-2x(10x^4 - 51x^3 - 93x^2 - 51x - 9)}{3x^4(1 + 2x)^3} + \frac{(x^2 - 2x - 3) \ln(2x + 1)}{x^4}. \quad (19)$$

For small x this can be expanded as a power series giving

$$F_{\text{loss}}(x) \approx \frac{8}{3} - \frac{56}{5}x + \frac{196}{5}x^2 - \frac{12928}{105}x^3 \dots \quad x \ll 1, \quad (20)$$

which is useful for numerical calculation.

We denote the average of $\dot{\gamma}_{\text{ic}}$ over an isotropic distribution of electron directions (or, equivalently, incoming photon directions) by

$$\langle \dot{\gamma}_{\text{ic}} \rangle = \frac{1}{2} \int_{-1}^1 d\cos \psi \dot{\gamma}_{\text{ic}} \quad (21)$$

which it is most convenient to evaluate numerically using equations (19) and (20). Alternatively, it can be written in the form

$$\langle \dot{\gamma}_{\text{ic}} \rangle = -\frac{4}{3} cN\sigma_{\text{T}} \gamma^2 \epsilon_0 G(\gamma, \epsilon_0) \quad (22)$$

where, after substituting Eq. (18) into Eq. (21) and reversing the order of the integrals over $\cos \psi$ and f , it can be shown that

$$G(\gamma, \epsilon) = \frac{9}{64\gamma^4\epsilon^3\beta} \{ \gamma[f_1(\epsilon\bar{\gamma}) - f_1(\epsilon/\bar{\gamma})] - \epsilon[f_2(\epsilon\bar{\gamma}) - f_2(\epsilon/\bar{\gamma})] \} \quad (23)$$

with $\bar{\gamma} = \gamma(1 + \beta) = \gamma + (\gamma^2 - 1)^{1/2}$ and

$$\begin{aligned} f_1(z) &= (z + 6 + 3/z) \ln(1 + 2z) - (22z^3/3 + 24z^2 + 18z + 4)(1 + 2z)^{-2} \\ &\quad - 2 + 2\text{Li}_2(-2z) \\ f_2(z) &= (z + 31/6 + 5/z + 3/2z^2) \ln(1 + 2z) - (22z^3/3 + 28z^2 + 103z/3 \\ &\quad + 17 + 3/z)(1 + 2z)^{-2} - 2 + 2\text{Li}_2(-2z) \end{aligned} \quad (24)$$

where the function $\text{Li}_2(z)$ is the Eulerian dilogarithm. This result was first derived by Jones [1965].

In the inverse Compton scattering regime, in which the energy of the incoming photon is negligible, the average energy of the scattered photon is

$$\bar{\epsilon}_{\text{ic}}(\gamma, \psi) = \frac{-\dot{\gamma}_{\text{ic}}}{N_{\text{ic}}} . \quad (25)$$

This photon is emitted in the direction of motion of the electron, and the emissivity – the number of photons emitted per second per electron in unit energy interval around ϵ – can be approximated by

$$\eta_{\text{ic}}(\epsilon, \gamma, \psi) = \dot{N}_{\text{ic}}(\gamma, \psi) \delta(\epsilon - \bar{\epsilon}_{\text{ic}}(\gamma, \psi)) , \quad (26)$$

[Felten & Morrison 1966].

Synchrotron radiation can be treated in an analogous manner [Hoyle 1960], using the ‘delta-function’ approximation in which it is assumed that all the emission from a given electron occurs at the energy $\bar{\varepsilon}_s(\gamma)$. The rate of change of the electron Lorentz factor due to synchrotron losses, averaged over pitch angle, is

$$\langle \dot{\gamma}_s \rangle = -\frac{4}{3} cN(R) \sigma_T \gamma^2 \epsilon_0 b^2 \quad (27)$$

and the pitch-angle averaged synchrotron emissivity per electron becomes

$$\begin{aligned} \eta_s(\varepsilon, \gamma) &= \dot{N}_s \delta(\varepsilon - \bar{\varepsilon}_s(\gamma)) \\ &= \frac{\langle -\dot{\gamma}_s \rangle}{\bar{\varepsilon}_s(\gamma)} \delta(\varepsilon - \bar{\varepsilon}_s(\gamma)) . \end{aligned} \quad (28)$$

The average frequency of the synchrotron photon is given by

$$\bar{\varepsilon}_s(\gamma) = \gamma^2 b \sqrt{\frac{\pi^3}{8} \frac{\epsilon_0 N r_0^3}{\alpha_f^2}} \quad (29)$$

where α_f is the fine-structure constant and r_0 the classical radius of the electron.

Substitution of the delta-function approximation (26) for the inverse Compton emissivity into Eq. (8) implies that the rate of emission of inverse Compton photons per steradian per second per energy interval is

$$\frac{dN_{ic}}{d\vec{\Omega}d\varepsilon dt} = n_e(\gamma_{ic}) \dot{N}_{ic}(\gamma_{ic}, \psi) \frac{d\gamma_{ic}}{d\varepsilon} . \quad (30)$$

The Lorentz factor $\gamma_{ic}(\varepsilon, \psi)$ of an electron which emits inverse Compton photons of energy ε is defined by the implicit relation $\varepsilon = \bar{\varepsilon}_{ic}(\gamma_{ic}, \psi)$.

Similarly, from (27) and Eq. (9), the rate of emission of synchrotron photons per steradian per second per energy interval is

$$\frac{dN_s}{d\vec{\Omega}d\varepsilon dt} = n_e(\gamma_s) \dot{N}_s(\gamma_s) \frac{d\gamma_s}{d\varepsilon} \quad (31)$$

where now the Lorentz factor γ_s of an electron which emits synchrotron radiation at energy ε is defined by $\varepsilon = \bar{\varepsilon}_s(\gamma_s)$, and from Eq. (29),

$$\gamma_s = \sqrt{\frac{\varepsilon}{b}} \left[\frac{\pi^3}{8} \frac{\epsilon_0 N_0 r_0^3}{\alpha_f^2} \right]^{-1/4} . \quad (32)$$

Appendix B: Opacity due to photon-photon pair production

The computation of the optical depth due to photon-photon pair production is most conveniently treated in the zero momentum frame, commonly referred to as the centre of momentum frame (CM frame) of the photon-pair [Jauch & Rohrlich 1976, Svensson 1982]. In the CM frame, the cross section is

$$\bar{\sigma} = \frac{\pi r_0^2}{2}(1 - \zeta^2) \left[(3 - \zeta^4) \ln \left(\frac{1 + \zeta}{1 - \zeta} \right) - 2\zeta(2 - \zeta^2) \right], \quad (33)$$

where $\zeta = \sqrt{\bar{\epsilon}^2 - 1}/\bar{\epsilon}$ and bars denote quantities measured in the CM frame in which each photon has an energy $\bar{\epsilon}$. The photon energy in the CM frame is related to the photon energies in the observer's frame through the invariant

$$E^2 - c^2 P^2 = 2(1 - \cos \psi) \epsilon_{ic} \epsilon = 4\bar{\epsilon}^2, \quad (34)$$

where E is the total energy and P is the magnitude of \vec{P} , the total momentum of the photon pair, and ψ is now the angle between the momentum vectors of the high-energy photon and the target photon in the observer's frame. The threshold condition is $\bar{\epsilon} > 1$.

The optical depth between two points on a photon trajectory is a Lorentz invariant, and is given by

$$d\tau = 2d\bar{r} \int d\bar{\epsilon} d\bar{\Omega} \bar{\sigma} \bar{n}_\gamma = 2d\bar{r} \int d\epsilon d\Omega \bar{\sigma} \frac{\bar{\epsilon}}{\epsilon} n_\gamma, \quad (35)$$

where $d\bar{r}$ is the spatial separation of the points in the CM frame. The factor 2 depends on the convention adopted for the definition of the cross section and stems from the fact that the relative speed of the photons in the CM frame is $2c$ [see Jauch & Rohrlich 1976]. The conversion from quantities in the CM frame to those in the observer's frame in (35) exploits the Lorentz invariance of n_γ/ϵ^2 and $\epsilon d\Omega d\epsilon$.

The line element in the CM frame is given by $d\bar{r} = dr\gamma_b(1 - \beta_b \cos \chi)$, where $\gamma_b = (1 - \beta_b^2)^{-1/2}$ is the Lorentz factor of the boost from the observer's frame to the CM frame and χ is the angle between the Lorentz boost and the ray path. Assuming monoenergetic target photons from the Be star (Eq. 4), it follows that

$$d\tau = N(R) \bar{\sigma}(\bar{\epsilon}) (1 - \cos \psi) dr, \quad (36)$$

where $N(R)$ is the number density of target photons at a distance R from the Be star (see Fig. 1).

There is a one-to-one correspondence between r along a given ray (i.e. for a given angle θ) and the energy, $\bar{\epsilon}$, of the photons in the CM frame. The optical

depth from the pulsar to the Earth, given by (35), may therefore be rewritten as an integral over the CM-frame photon energy instead of the coordinate along the ray r . Substituting $\alpha = \bar{\epsilon}/\sqrt{\epsilon_{\text{ic}}\epsilon_0}$ one finds

$$\tau(\epsilon_{\text{ic}}, \theta) = \frac{4N_0 D}{\sin \theta} \int_{1/\sqrt{\epsilon_{\text{ic}}\epsilon_0}}^{\sqrt{(1+\cos \theta)/2}} d\alpha \frac{\alpha^2}{\sqrt{1-\alpha^2}} \bar{\sigma}(\alpha\sqrt{\epsilon_{\text{ic}}\epsilon_0}) . \quad (37)$$

The upper limit of the integral in (37) corresponds to the position of the pulsar. Pair production is only possible if the energy of the photon exceeds the threshold Eq. (10). As ψ becomes small at a large distances from the star, pair production ceases at some finite point. The lower limit of the integral in (37) corresponds to this cut-off.

References

- [1] Ball, L., Melatos, A., Johnston, S., Skjæraasen, O., 1998, ApJL, submitted
- [2] Bell, J. F., Bessell, M. S., Stappers, B. W., Bailes, M., Kaspi, V. M., 1995, ApJ, 447, L117
- [3] Blumenthal, G. R., Gould, R. J., 1970, Rev. Mod. Phys., 42, 237
- [4] Blumenthal, G. R., 1971, Phys. Rev. D, 3, 2308
- [5] Cominsky, L., Roberts, M., Johnston, S., 1994, ApJ, 427, 978
- [6] De Jager, O. C., Harding, A. K., 1992, ApJ, 396, 161
- [7] Felten, J.E., Morrison, P., 1966, ApJ, 146, 686
- [8] Grove J. E., Tavani M., Purcell W. R., Johnson W. N., Kurfess J. D., Strickman M. S., Arons J., 1995, ApJ, 447, L113
- [9] Harding, A. K., 1996, Space Sc. Rev., 75, 257
- [10] Hirayama, M., Nagase, F., Tavani, M., Kaspi, V. M., Kawai, N., Arons, J., 1996, PASJ, 48, 833
- [11] HEGRA Collaboration, 1996, Astroparticle Phys., 4, 199
- [12] Hoyle, F., 1960, MNRAS, 120, 338
- [13] Jauch, J. M., Rohrlich, F., *The theory of photons and electrons*, Springer Verlag, 1976
- [14] Johnston, S., Manchester, R. N., Lyne, A. G., Bailes, M., Kaspi, V. M., Qiao, G., D'Amico, N., 1992, ApJ, 387, L37

- [15] Johnston, S., Manchester, R. N., Lyne, A. G., Nicastro, L., Spyromilio, J., 1994, MNRAS, 268, 430
- [16] Johnston, S., Manchester, R. N., Lyne, A. G., D’Amico, N., Bailes, M., Gaensler, B. M., Nicastro, L., 1996, MNRAS, 279, 1026
- [17] Johnston, S., Manchester, R. N., McConnell, D., Campbell-Wilson, D., 1998, MNRAS, submitted
- [18] Jones, F. C., 1965, Phys Rev B, 137, 1306
- [19] Kaspi, V. M., Johnston, S., Bell, J. F., Manchester, R. N., Bailes, M., Bessell, M., Lyne, A. G., D’Amico, N., 1994, ApJ, 423, L43
- [20] Kaspi, V. M., Tavani, M., Nagase, F., Hirayama, M., Hoshino, M., Aoki, T., Kawai, N., Arons, J., 1995, ApJ, 453, 424
- [21] Kawachi, A., 1997, Proc. neutron stars and pulsars, Rikkyo University, Japan, Universal Academy Press, Tokyo, Japan, in press
- [22] Kennel, C. F., Coroniti, F. V., 1984, ApJ, 283, 710
- [23] Kifune, T., et al., 1995, ApJ, 438, L91
- [24] Kifune, T., 1997, Proc. Kruger Workshop “Towards a major atmospheric Cherenkov telescope V”, in press
- [25] Mastichiadis, A., 1991, MNRAS, 253, 235
- [26] Melatos, A., Johnston, S., Melrose, D. B., 1995, MNRAS, 275, 381
- [27] Rees, M. J., Gunn, J. E., 1974, MNRAS, 167, 1
- [28] Sako, T., et al., 1997, Proc. 25th ICRC (Durban), 3, 165
- [29] Svensson, R., 1982, ApJ, 258, 335
- [30] Tanimori, T., et al., 1998, ApJ, 492, L33
- [31] Tavani, M., et al., 1996, A&AS, 120, 221
- [32] Tavani, M., Arons, J., 1997, ApJ, 477, 439
- [33] Underhill, A., Doazan, V., 1982, ‘B stars with and without emission lines’, NASA SP-456
- [34] Vacanti, G., et al., 1991, ApJ, 377, 467
- [35] Yoshikoshi, T., et al., 1997, ApJ, 487, L65